

# SYNTHESIS AND CHARACTERISATION OF W-, Ag-, AND W/Ag- CO-DOPED TITANIA NANOPOWDERS, AND THEIR PHOTOCATALYTIC ACTIVITY

João Antonio Labrincha<sup>1,\*</sup>, David Maria Tobaldi<sup>1</sup>, Maria Paula Seabra<sup>1</sup>, Robert Carlyle Pullar<sup>1</sup>, Clara Piccirillo<sup>2</sup>

Received: August 22, 2012; Revised: July 15, 2013; Accepted: July 15, 2013

## Abstract

Tungsten, silver, and tungsten/silver co-doped titania nanopowders were synthesised via an aqueous sol-gel method. The dried gels were thermally treated at 2 different temperatures, and the occurrence of the amorphous phase was assessed, using the combined Rietveld-RIR method, on the X-ray powder diffraction data. Systematic studies of the crystal structure and of the optical properties of the powders – made with diffuse reflectance spectroscopy (DRS) – were performed. The energy band gap was calculated using the differential reflectance method; their morphology was investigated using field emission scanning electron microscopy and transmission electron microscopy analyses (FE-SEM and TEM, respectively). The photocatalytic activity of the samples was assessed in liquid-solid phase, under UVA-light and visible-light irradiation, monitoring the degradation of an organic dye. The influence of the phase composition, optical properties, dimensions, and specific surface area of the powders on the photocatalytic activity was thoroughly discussed.

**Keywords:** Sol-gel synthesis, nanostructures, X-ray diffraction, optical properties, doped titania, photocatalysis

## Introduction

Titanium dioxide (TiO<sub>2</sub>) crystallises in a large number of polymorphs: the high-pressure columbite-like (Haines and Leger, 1993), baddeleyite-like (Sato *et al.*, 1991), and cotunnite-like (*c*-TiO<sub>2</sub>) structures (Dubrovinsky *et al.*, 2001), exist besides the well-known – in order of abundance – rutile, anatase, and brookite phases (Muscat *et al.*, 2002). TiO<sub>2</sub> is a common and widely used material in everyday life applications, not only for its well-established use in paints, as a whitening agent for food, and in personal care products or pharmaceuticals (Weir *et al.*, 2012), but also for its use in electrochemical electrodes

---

<sup>1</sup> *Materials and Ceramics Engineering Department / CICECO, University of Aveiro, Campus Universitário de Santiago, 3810-193 Aveiro, Portugal. Tel.: +351 234 370 041; E-mail: jal@ua.pt*

<sup>2</sup> *CBQF/Escola Superior de Biotecnologia, Universidade Católica Portuguesa, R. Dr. António Bernardino de Almeida, 4200-072 Porto, Portugal.*

\* *Corresponding author*

and solar cells (O'Regan and Grätzel, 1991). In particular, in recent decades, TiO<sub>2</sub> has been experiencing more and more attention after the discovery, in 1972, of the so-called "Honda-Fujishima effect" (Fujishima and Honda, 1972). This was photo-electrochemical water splitting, using a single-crystal titania electrode. As a result, in recent decades the degree of interest in semiconductor photocatalysis has grown exponentially, not only in the areas of water and air purification (Chen and Poon, 2009; Puddu *et al.*, 2010), but also in wastewater treatment (Malato *et al.*, 2009). Semiconductors (*e.g.* TiO<sub>2</sub>, ZnO,  $\alpha$ -Fe<sub>2</sub>O<sub>3</sub>, or CdS) are able to act as sensitizers for light-activated redox processes because of their electronic structure: when a photon matches or exceeds the band gap energy of the semiconductor, an electron is liberated from the valence band into the conduction band, leaving a hole behind (Hoffmann *et al.*, 1995). The photo-generated pair (e<sup>-</sup>-h<sup>+</sup>) is able to reduce and oxidise a pollutant that is adsorbed on the photocatalyst surface (Fujishima *et al.*, 2000). Amongst semiconductors, TiO<sub>2</sub> is indeed the most investigated photocatalytic material. TiO<sub>2</sub> is chemically inert and non-toxic; the reactions take place under mild operating conditions (*e.g.* a low level of solar or artificial illumination, room temperature (RT), and atmospheric pressure); no chemical additive is necessary; the possible intermediates of the reactions are not dangerous (or at least are less dangerous than the original pollutant) (Arsac *et al.*, 2008); and even very recalcitrant and persistent pollutants can be degraded (Herrmann *et al.*, 2007). Moreover, one peculiar characteristic of TiO<sub>2</sub> – simultaneous with the photocatalytic activity – is its antibacterial activity. When irradiated with light with a wavelength greater than the band-gap, TiO<sub>2</sub> photocatalysts can also be used to inactivate or kill bacteria that are on the photocatalyst surface, and hence to make those surfaces self-sterilising (Fujishima *et al.*, 1999).

Amongst TiO<sub>2</sub> polymorphs, anatase and rutile are the most utilized in photocatalytic applications, although anatase is considered to be more photoactive than rutile (Ohno *et al.*,

2001), because of its stronger reducing power and better hole-trapping ability (Augustynski, 1993). Anatase and rutile are wide band gap semiconductors – their band gap is equal to 3.23 and 3.02 eV, respectively – and this means that the photocatalytic reaction is promoted by light having UVA radiation. Consequently, titania exploits only 3–5% of the available solar energy in the photocatalytic reaction, being transparent for most of the solar radiation spectrum (Karvinen and Lamminmäki, 2003).

A possible means of extending the photocatalytic activity of titania into the visible region is doping it with transition metals (Choi *et al.*, 1994; Fuente *et al.*, 2001). In particular, the doping of TiO<sub>2</sub> with WO<sub>3</sub> is able to improve the TiO<sub>2</sub> photocatalytic activity in several ways: it prevents the recombination of the electron-hole pairs (e<sup>-</sup>-h<sup>+</sup>) (Tatsuma *et al.*, 2001), it may shift the light absorption band from the UVA to the visible region (Li *et al.*, 2001), and it is able to increase the surface acidity of the photocatalyst; hence it can absorb more hydroxyl groups and, simultaneously, more organic reactants on its surface (Kwon *et al.*, 2000). Furthermore, noble metal modification improves the photocatalytic activity of titania by accelerating liquid-solid photocatalytic reactions (Sakthivel *et al.*, 2004), and by reducing the fast recombination of the photo-generated e<sup>-</sup>-h<sup>+</sup> charge carriers (Kominami *et al.*, 2002). Amongst noble metals, silver is particularly attractive due to its remarkable catalytic activity (Jana *et al.*, 1999), its size-, as well as shape-dependent optical properties (Wang and Herron, 1991; Jin *et al.*, 2003), its possible applications in biological and chemical sensing due to its localised surface plasmon resonance (Hutter *et al.*, 2001); and also because of its long-established, well-known antibacterial properties, due to the so-called "oligodynamic effect" (Lansdown, 2010).

In this work, W-doped, Ag-doped, and W/Ag-co-doped titania were successfully synthesised via the sol-gel technique. The phase composition and crystal structure – by means of X-ray powder diffraction (XRPD)

and the Rietveld method – as well as the optical properties of the prepared samples, were thoroughly investigated. The photocatalytic activity – assessed in liquid-solid phase, by monitoring the degradation of an organic dye, under UVA-light and visible-light irradiation – of the samples was also tested. Results were explained taking into account the effects which the variation of crystallinity, crystalline phase, and optical and physical properties might exert on the photocatalytic activity of the samples.

## Experimental

### Sample Preparation

Aqueous titanium(IV)hydroxide sols were made from the peptisation of hydrolysed titanium (IV) isopropoxide (Ti-*i*-pr, Ti (OCH(CH<sub>3</sub>)<sub>2</sub>)<sub>4</sub>), using distilled water. One part of Ti-*i*-pr (Aldrich, 97%) was added to 4 parts of isopropyl alcohol (IPA, propan-2-ol) to make a 20% Ti-*i*-pr solution. This Ti-*i*-pr solution was hydrolysed by the dropwise addition of an excess of water (5:1 water: Ti-*i*-pr) as a 20% solution in IPA. The acid necessary to peptise the sol was also added to this water-IPA solution – concentrated HNO<sub>3</sub> (Aldrich, 65%, Sigma-Aldrich Corp., St. Louis, MO, USA), added in a ratio of Ti<sup>4+</sup>:HNO<sub>3</sub> of 5:1. This water-IPA-HNO<sub>3</sub> solution was added dropwise to the Ti-*i*-pr solution at RT, whilst it was mechanically stirred at 800-1200 rpm. The precipitated mixture was evaporated to a white jelly-like mass on a rotary evaporator at 60°C and 140 mPa. Distilled water was added to restore the mixture to the original volume, the gelatinous mass was redispersed in a few minutes, and the solution evaporated to a jelly-like mass again, this time at 65 mPa and 60°C. This time when water was added again, the gelatinous mass dispersed to form a sol in 2 min, and the sol was diluted to a concentration of 1 M Ti<sup>4+</sup>.

To make the 1 mol% W<sup>6+</sup> and Ag<sup>+</sup> doped sols, stoichiometric amounts of silver nitrate (1 M aqueous solution, Aldrich) or tungstic acid (WH<sub>2</sub>O<sub>4</sub> powder, Aldrich) were added to

the sol. In the case of Ag<sup>+</sup>, the AgNO<sub>3</sub> solution was directly added to the peptised sol, when the sol had a 1 M concentration. With W<sup>6+</sup>, the process is much more complicated, and differed from the standard Ti sol preparation. WH<sub>2</sub>O<sub>4</sub> is soluble in concentrated ammonia solution, not water or IPA. Therefore, a stoichiometric amount of WH<sub>2</sub>O<sub>4</sub> (0.5 g) was dissolved in a slight excess of concentrated ammonia (12 ml of 25% NH<sub>3</sub> solution). This was then added to 20 g water, and to this was then added 70 ml of IPA. A very slight cloudiness could be observed as the aqueous and IPA liquids mixed, which could indicate that some of the WH<sub>2</sub>O<sub>4</sub> was precipitated by the IPA, but this seemed to dissipate after time, and the burette used to add the aqueous solution never became blocked by a solid. This aqueous solution was then added dropwise to a 20% Ti-*i*-pr solution (20% in IPA) with mechanical stirring, as above, although obviously this time without the addition of any acid to the highly basic mixture. As above, the IPA was removed on a rotary evaporator, and then replaced with water, which in this case had HNO<sub>3</sub> added. A higher ratio of 1.25:1 (5:4) Ti<sup>4+</sup>:HNO<sub>3</sub> was needed, probably due to some ammonia remaining in the dried gel. This was again evaporated to a gel, and then redispersed in more added water to form a sol in 30 min. The 1.0 mol% Ag<sup>+</sup> / 1.0 mol% W<sup>6+</sup> co-doped sol was made from a W<sup>6+</sup> doped sol made as above. To this sol, the stoichiometric amount of AgNO<sub>3</sub> was added afterwards. All sols were maintained at a 1M concentration, and were shown to be stable for over a week in all cases, and often several weeks. The volume of solvent/water before evaporation on the rotary evaporator was approximately 500 ml in all cases.

The as-synthesised gels were dried in an oven at 80°C, and afterwards the dried gels were thermally treated at 450°C and 600°C in a static air flow. The thermal rate, from RT to the maximum temperature, was 5°C min<sup>-1</sup>, followed by 2 h of soaking time. Undoped titania samples were referred to by Ti450 and Ti600 symbols, where the number represents the 2 maximum firing temperatures reached;

doped gels were instead indicated by adding the W- or Ag- chemical symbols; when co-doped, W/Ag- was the symbol added.

### Sample Characterisation

The unit cell parameters of the prepared samples were determined using LaB<sub>6</sub> (National Institute of Science and Technology 660b) as the internal standard. XRPD data were collected by using a  $\theta/2\theta$  diffractometer, Panalytical X'Pert Pro (PANalytical B.V., Almelo, Netherlands), equipped with a fast remote traffic microwave sensor (RTMS) detector, with graphite monochromated Cu K $\alpha$  radiation (40kV and 40 mA, 20°-80° 2 $\theta$  range, a virtual step scan of 0.0167° 2°, and 50 s per step). Divergence and anti-scattering slits of 0.125° and 0.125°, respectively, were mounted in the incident beam pathway. The pathway of the diffracted beam included a Ni filter, a soller slit (0.01 rad), and an antiscatter blade (5 mm). The full profile fitting analyses were performed using XRPD data, and Rietveld refinements were accomplished with the general structure analysis system (GSAS) (Larson and Von Dreele, 2000) package and its graphical interface EXPGUI (Toby, 2001). The starting atomic parameters for anatase and rutile, described in the space groups  $I4_1/amd$  and  $P4_2/mnm$  respectively, were taken from Howard *et al.* (1991); brookite ones, described in the space group  $Pbca$ , were obtained from Meagher and Lager (1979). In the full Rietveld refinements, these parameters were refined: scale-factors, zero-point, the background signal modelled using a 6<sup>th</sup>-order of the shifted Chebyshev polynomial function, unit cell parameters and profile coefficients – 1 Gaussian ( $G_w$ ), an angle-independent term, and 2 Lorentzian terms,  $L_x$  and  $L_y$  – peak correction for asymmetry, and sample displacement effects. For all XRPD measurements, the samples were carefully ground and mounted in aluminum sample holders using a side-loading technique. XRPD data were also used for the quantitative phase analysis (QPA). Data were collected using a  $\theta/\theta$  diffractometer, Panalytical X'Pert

Pro, equipped with a fast RTMS detector, with graphite monochromated Cu K $\alpha$  radiation (40 kV and 40 mA, 20-80  $2\theta$  range, a virtual step scan of 0.0167  $2\theta$ , and virtual time per step of 50s). Divergence and anti-scattering slits of 0.125° and 0.125°, respectively, were mounted in the incident beam pathway. The pathway of the diffracted beam included a Ni filter, a soller slit (0.01 rad), and an antiscatter blade (5 mm). Full QPA (*i.e.* determination of both the crystalline and amorphous content) was performed using the combined Rietveld–RIR method (Gualtieri, 2000; Gualtieri and Brignoli, 2004): 10 wt% corundum (National Institute of Science and Technology 676a) was added to the sample, and treated as an additional phase in the refinements. In this case, the refined weight fractions of each crystalline phase ( $X_{ic}$ ) were rescaled with respect to the known weight fraction of the added standard ( $X_s$ ) in order to obtain the real crystalline phase weight fraction ( $X_i$ ):

$$X_i = \frac{1}{1 - X_s} \left[ \left( \frac{X_s}{X_{sc}} \right) X_{ic} \right] \quad (1)$$

where  $X_{sc}$  is the refined weight fraction of the internal standard. Knowing the weight fractions of all crystalline phases, the amorphous content ( $X_a$ ) is calculated using the following equation:

$$X_a = 1 - \sum_i X_i \quad (2)$$

DRS was performed with a Shimadzu UV 3100 (Shimadzu Corp., Kyoto, Japan) spectrometer and spectra of the samples were acquired in the UV-Vis range (250-750 nm), with 0.02 nm in step-size and using BaSO<sub>4</sub> as the reference. The Kubelka-Munk function was applied with the aim of converting the diffuse reflectance into the absorption coefficient  $\alpha$ :

$$\alpha \approx \frac{K}{S} = \frac{(1 - R_\infty)^2}{2R_\infty} \equiv F(R_\infty) \quad (3)$$

where  $K$  and  $S$  are the absorption and scattering coefficients; the reflectance  $R_\infty$

is equal to  $R_{\text{sample}}/R_{\text{standard}}$  (Marfunin, 1979).

The energy band gap ( $E_g$ ) of the powders was calculated using the differential reflectance method (a method mainly applied for well-crystalline semiconductor materials). This method assumes that, plotting the first derivative of reflectance ( $dR/d\lambda$ ) versus the wavelength ( $\lambda$ ), the maximum value of such a plot corresponds to the band gap of the semiconductor material (Komornicki *et al.*, 2004).

The morphology of the samples was investigated by TEM (Hitachi H9000, Hitachi Ltd., Tokyo, Japan), equipped with an energy dispersive x-ray spectroscopy (EDS) attachment (Bruker Quantax 400, Bruker Corp., Billerica, MA, USA), and FE-SEM (Hitachi SU-70, JP). The specific surface area (SSA) of the prepared samples was evaluated by the Brunauer-Emmett-Teller method (Micromeritics Gemini 2380, Micromeritics Instrument Corp., Norcross, GA, USA), using  $N_2$  as the adsorbate gas.

### Evaluation of Photocatalytic Activity

The photocatalytic activity of the prepared powders was evaluated in liquid-solid phase, monitoring the degradation of an organic dye – methylene blue (MB, Aldrich) – using a spectrometer (Shimadzu UV 3100, JP). The tests were performed at RT, in a cylindrical photocatalytic reactor (100 mm in diameter) containing an aqueous solution of the dye (1 L), at an initial concentration of 5 mg L<sup>-1</sup>. The concentration of the photocatalyst in the slurry was 0.25 g L<sup>-1</sup>. In order to mix the solution thoroughly, the slurry was magnetically stirred throughout the reaction; the reactor was covered with a watch-glass, so as to avoid the evaporation of the solution. The lighting of the reacting system was assured by placing 2 lamps at either side of the reactor; the distance between the lamps and the reactor was 5 cm. The UVA-light source was a germicidal lamp (Philips PL-S 9W, Koninklijke Philips N.V., Eindhoven, Netherlands), having an irradiance of approximately 13 W m<sup>-2</sup> in the UVA range; while the visible-light source was a

fluorescent lamp (Philips master PL-S 2P 9W/840, NL), having an irradiance of ~50 W m<sup>-2</sup> in the visible region and 600×10<sup>-3</sup> W m<sup>-2</sup> in the UVA region. In the experiments, the photocatalytic degradation of the MB was monitored by sampling about 4 mL of the slurry from the reactor, at regular time intervals. Before switching the lamps on, the suspension was stirred in the dark for 30 min, with the aim of allowing the adsorption of MB onto the powders. The powders in the samples were separated by centrifugation, and then the MB concentration in the liquid was determined, taking advantage of the Lambert-Beer law, by measuring the absorbance in a spectrometer at a wavelength of 665 nm, using distilled water as a reference. The photocatalytic reaction is a pseudo first-order reaction, hence, the extent of MB degradation was evaluated as the apparent first-order constant ( $k'_{\text{app}}$ ):

$$\ln\left(\frac{C_0}{C}\right) = k'_{\text{app}} t \quad (4)$$

where  $C_0$  is the initial concentration of orange II (OII) and  $C$  is its concentration after a certain UVA- visible-light irradiation time  $t$ . The plot of  $\ln\left(\frac{C_0}{C}\right)$  Vs the irradiation time, gives a straight line, whose slope corresponds to the value of the pseudo first-order apparent rate constant ( $k'_{\text{app}}$ ) (Al-Ekabi and Serpone, 1988). Commercial Aeroxide® TiO<sub>2</sub> P25 photocatalytic powder (Evonik Industries, Essen, Germany) was used for comparison.

## Results and Discussion

### Morphology of the Fired Powders

The fired powders consist of poorly crystallised, strongly aggregated, and sub-spherical-shaped particles, as shown by TEM analysis (Figure 1(a-d)). Undoped TiO<sub>2</sub> particles possess a broad particle size distribution, with dimensions ranging from tens of nanometres, up to ~50 nm (Figure 1(a)). W-doping gives the

powders a narrower grain size distribution, if compared to the undoped ones, and the mean particle size decreases as well (Figure 1(b)). Also the Ag-doped powders, at 450°C, possess a wide particle size distribution (Figure 1(c)); it is seen as well that an increase of firing temperature causes a growth in particle size. Moreover, in the Ag-doped sample fired at 600°C, rounded nanoscale Ag particles that are clustered around the larger titania ones, are clearly visible (Figure 1(d)).

### X-ray Diffraction Analysis

The powder diffraction patterns of the samples that were dried in an oven at 120°C (data were not reported here) interestingly show that, already at this temperature and with this synthesis method, poorly crystalline anatase, rutile, and brookite – at different amounts within the prepared powders – coexisted with the amorphous phase, and

well-crystalline titanium hydrogen oxide hydrate. The powder diffraction patterns of the samples fired at 450°C are depicted in Figure 2(a). In these, the presence of W and/or Ag oxides was not detected. The incorporation of W into the titania lattice is predictable – the effective ionic radii of  $^{61}\text{Ti}^{4+}$  and  $^{61}\text{W}^{6+}$  are 0.61 and 0.60 Å, respectively (Shannon, 1976). On the other hand, the incorporation of Ag into the titania lattice is not likely (as was demonstrated by TEM observations), the  $^{61}\text{Ag}^+$  ionic radius being 1.15 Å (Shannon, 1976). Thus, we deem that its amount in the mixtures (1 mol%), is lower than the x-ray detection limit.

From the QPA data (Table 1), it can be inferred that samples fired at this temperature (450°C) had quite a large amount of amorphous phase (values ranging from 21.6 wt%, to 27.3 wt%), a legacy of the un-crystallised titania in the starting sols.

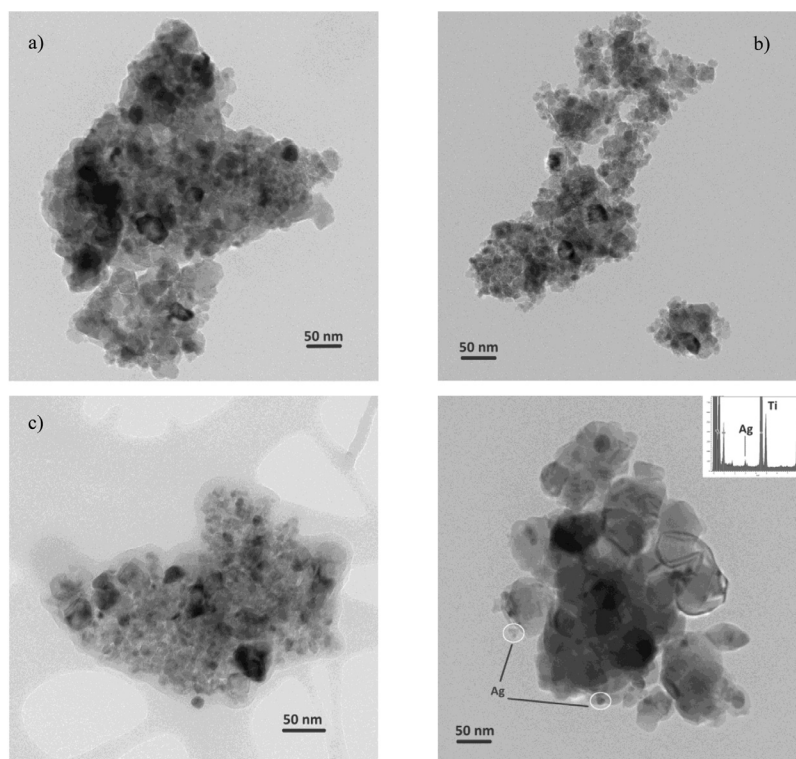


**Figure 1.** TEM micrographs of: a) sample Ti450; b) sample W-Ti450; c) Ag-Ti450; d) Ag-Ti600: the white circles indicate Ag nanoparticles, while the inset represents EDS analysis of them

**Table 1. Refinement parameters and phase composition of the undoped and doped titania samples. The phase composition was calculated from the Rietveld refinements of XRD patterns, using the NIST 676a internal standard**  
*There were 3528 observations for every refinement; the number of anatase, rutile, and brookite reflections was: 32, 31, and 154, respectively.*

Sample	Figures-of-merit				Phase composition			
	No. of variables	$R^2_F$	$R_{wp}$	$\chi^2$	anatase (wt%)	rutile (wt%)	brookite (wt%)	amorphous (wt%)
Ti450	25	0.03	0.05	1.4	25.1±0.1	37.7±0.1	10.3±0.4	26.9±0.7
W-Ti450	23	0.03	0.05	1.5	26.8±0.1	36.7±0.1	10.7±0.3	25.7±0.6
W/Ag-Ti450	18	0.04	0.06	1.7	1.7±0.1	76.8±0.1	–	21.6±0.3
Ag-Ti450	25	0.02	0.05	1.2	33.7±0.1	25.3±0.1	13.7±1.0	27.3±1.3
Ti600	20	0.05	0.07	2.0	1.3±0.1	73.9±0.1	–	24.8±0.3
W-Ti600	21	0.06	0.06	1.5	13.4±0.1	61.4±0.1	–	25.2±0.3
W/Ag-Ti600	16	0.08	0.06	1.9	0.7±0.1	80.0±0.1	–	19.3±0.3
Ag-Ti600	18	0.06	0.06	1.4	6.1±0.1	75.7±0.1	–	18.2±0.3

The relative amount of the brookite phase is approximately the same in all the samples. The co-doped sample was the only exception, having no brookite, its composition being: 1.7 wt% anatase, 76.8 wt% rutile, and 21.6 wt% amorphous phase. Thus, the co-doping concentration – 1 mol% – favours brookite  $\rightarrow$  rutile, and the anatase-to-rutile phase transformation (ART), at only 450°C. It has been reported that the ART mechanism changes with the Ag concentration (Chao *et al.*, 2003), hence, an addition of 0.5 mol% Ag might favour rutile formation at the expense of brookite. Moreover, the reference sample (Ti450) and the W-doped one (W-Ti450), had virtually the same phase composition. On the other hand, Ag addition delayed the ART: this sample contained 33.7 wt% anatase, 25.3 wt% rutile, and 13.7 wt% brookite. Actually, there exist many contradictory reports on the crystallisation and phase transition of titania doped with silver. For instance, Chao *et al.* (2003) reported that Ag insertion favoured the ART; on the contrary, according to García-Serrano *et al.* (2009), Ag incorporation inhibited the ART in TiO<sub>2</sub> nanoparticles. Essentially, crystallisation and, consequently, the ART, are affected by several parameters, such as: the synthesis process, the starting materials, atmosphere, and the presence of impurities or doping species. Hence, we can assume that with this synthesis method, at a rather low temperature of 450°C, the Ag insertion increased the thermal stability of the anatase nanoparticles, hindering the crystallisation process and shifting the ART toward higher temperatures.

The increase of the firing temperature leads to a disappearance of brookite in all the samples: at 600°C, the only crystalline phases are anatase and rutile, (Figure 2(b) and Table 1). The amount of the amorphous phase in samples Ti600 and W-Ti600 slightly decreased, if compared to the same samples fired at 450°C. Sample Ti600 had a marked ART, its anatase content being equal to 1.3 wt%. Ag- and co-doped samples had, instead, a lower amount of the amorphous

phase, namely, 18.2 and 19.3 wt%. Doping apparently favoured rutile formation, and accelerated the ART. Tungsten was the most effective in delaying the ART (anatase and rutile amounts in the W-doped sample were 13.4 wt% and 61.4 wt%, respectively). Actually, the incorporation of cations with a valence higher than 4+ into the anatase lattice is believed to retard the ART, due to the reduction of the oxygen vacancies and formation of interstitial Ti<sup>3+</sup>, thus repressing the atomic transfer in the anatase structure (Okada *et al.*, 2001). Hence, we assume that the reactions amorphous / brookite  $\rightarrow$  rutile, and anatase  $\rightarrow$  rutile, occurred at a higher temperature, and the nanocrystals of brookite rapidly transformed into rutile, because of their high activation energy (Zhang and Banfield, 2000).

Considering the unit cell parameters, the insertion of tungsten leads to an expansion of the anatase lattice, both at 450 and 600°C (Figure 3(a,b)). On the other hand, the W/Ag- and Ag- doping virtually did not modify the anatase lattice of the powders fired at 450°C; on the contrary, at 600°C, the Ag- and the co-doping led to a contraction of the anatase lattice. Taking into account the modification that doping exerted on the rutile lattice (Figure 3(c)), tungsten and co-doping led to an expansion of the rutile lattice in the powders fired at 450°C; Ag-doping, virtually did not modify its lattice, confirming the aforementioned assumption that the incorporation of Ag into the titania lattice is not likely, because of ionic radii issues. Referring to the rutile in the powders fired at 600°C (Figure 3(d)), its lattice is virtually the same as the one of the W- and W/Ag-doped samples, while, at this firing temperature, the Ag-doping led to a contraction of the rutile lattice, as also in the case of anatase.

### Optical Properties

The DRS of the synthesised powders are depicted in Figure 4(a) and (b). As expected, the undoped sample showed no absorption in the visible region. Its spectrum, at both firing temperatures, consisted of a single

absorption band, below approximately 410 nm, ascribed to the metal-ligand charge transfer in titania. Doped and co-doped samples (stored in the dark), besides that band, also showed an absorption tail in the visible region, at approximately 430 nm, at both firing temperatures. The exception was the co-doped sample fired at 600°C, in which the thermal treatment led to a disappearance of that absorption tail (Figure 4(b)).

The energy band gaps of the powders were calculated by the differential reflectance method (Table 2). The resulting curves were successfully fitted with a Gaussian function, and the maximum values were found from the fitting. The subsequent band gap energies of the samples were all assigned to rutile, since they are consistent with its expected  $E_g$  value, that is 3.02 eV (411 nm), referred to Table 2. Exceptions were the Ag-doped and the co-doped samples, at both the firing temperatures. These samples also showed a shoulder, centred at approximately 423 nm (2.93 eV), that can be attributed to Ag mid-gap states, that are in the titania forbidden band. In particular, silver doping creates middle Ag  $4d$  states, whose transitions between Ti  $3d$  states are the source of the visible absorption (Guo and Du, 2012).

### Photocatalytic Activity

Photocatalytic activity results, reported as the relative pseudo first-order apparent rate constant ( $k_{app}$ ) during the reactions – under UVA and visible-light exposure – are depicted in Figure 5(a-d).

Under UVA light irradiation, the reference sample, Aeroxide® TiO<sub>2</sub> P25 powder, had the best photocatalytic activity of all the sets of powders, fired both at 450 and 600°C, leading to a full degradation of the dye, in approximately 4 h of irradiation time (Figure 5(a), and (b)). Undoped sample Ti450 was the best photocatalyst amongst the synthesised powders fired at 450°C, leading almost to a complete degradation of the dye after 7 h of irradiation time (Figure 5(a)). Between the doped and co-doped samples, W-Ti450 had the better photocatalytic activity, followed by the co-doped sample and the Ag-doped one. In this case, dopants should behave as electron-hole recombination centres (Serpone *et al.*, 1994; Scalfani and Herrmann, 1998; Di Paola *et al.*, 2002). Moreover, the amount of amorphous phase also has to be taken into account, lowering the relative photocatalytic active centres on such samples (Tobaldi *et al.*, 2010). The increase of the firing temperature to 600°C, Figure 5(b),

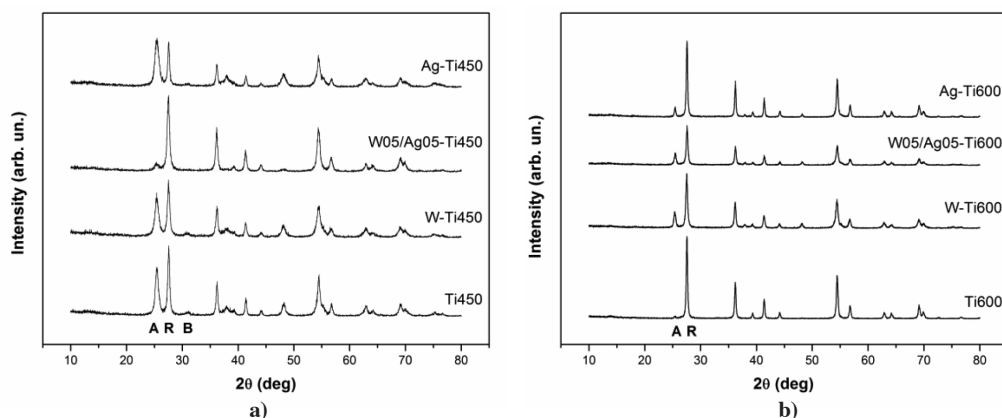


Figure 2. XRD patterns of the samples fired at: a) 450°C; b) 600°C. A, R, and B are symbols, standing for: anatase, rutile, and brookite, respectively

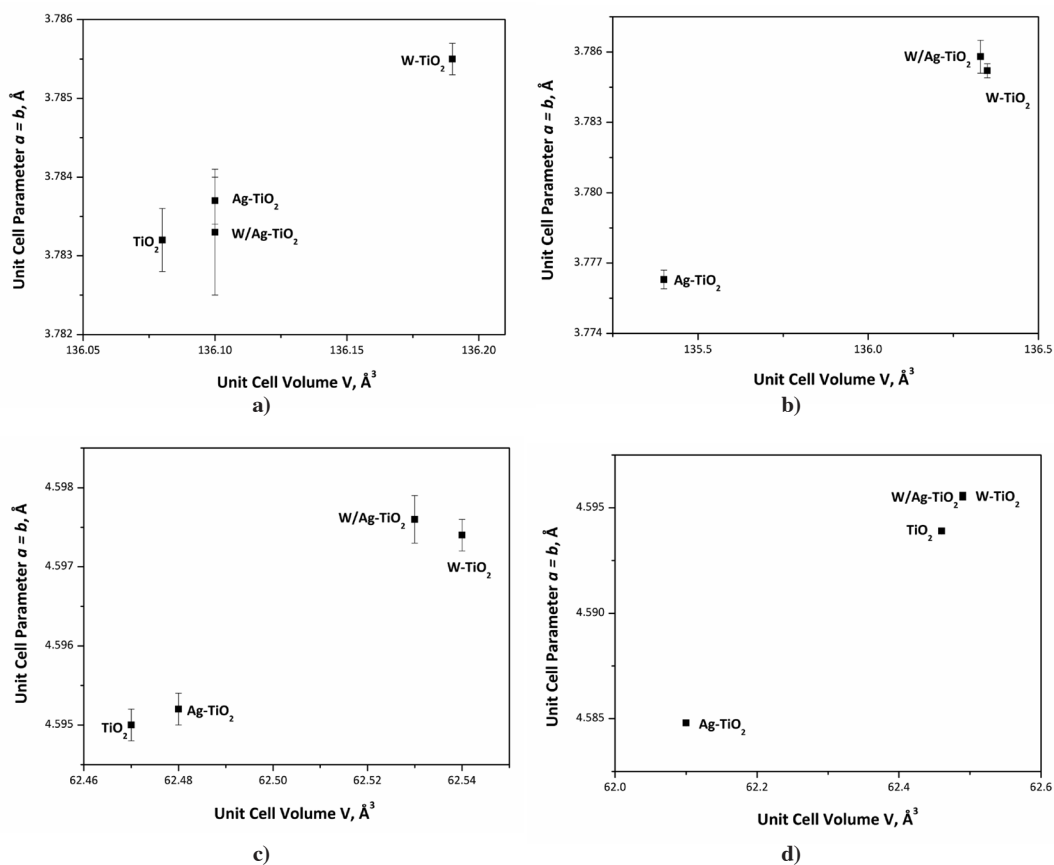


Figure 3. Unit cell parameters ( $a = b$ ) Vs unit cell volume of: a) anatase fired at 450°C; b) anatase fired at 600°C; c) rutile fired at 450°C; d) rutile fired at 600°C

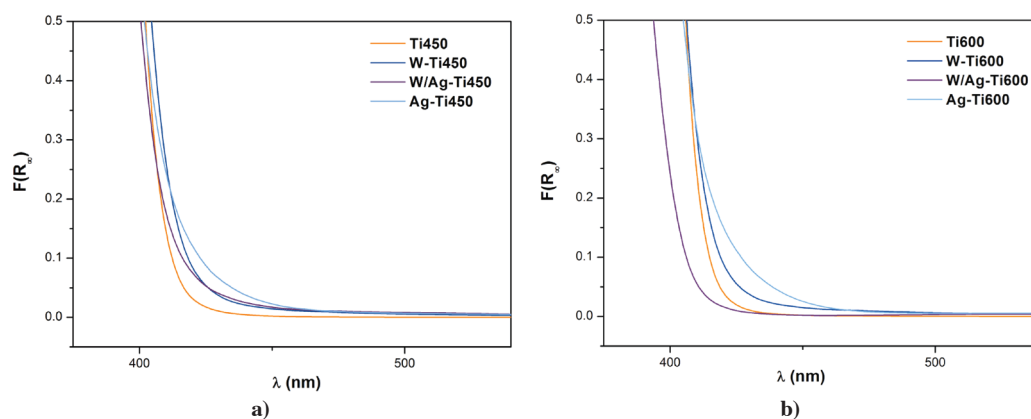


Figure 4. Diffuse reflectance spectra – in the  $\lambda$  range of 375-550 nm – of the samples fired at: a) 450°C, and b) 600°C

led to a decrease of the photocatalytic activity of all the tested samples. Such a decrease was more marked for the undoped and the Ag-doped samples with the lowest SSA. On the contrary, the photocatalytic activity of the W- and co-doped samples did not suffer dramatically with the increase of firing temperature. Actually, the W- and co-doped samples are the ones with the highest SSA values at this firing temperature, and this made such behaviour possible.

Visible-light exposure led to a lowering of the overall photocatalytic performance, even if every sample was shown to be active at both firing temperatures. Furthermore, their photocatalytic activity (the only exception being sample Ag-Ti600) was higher than that of the Aeroxide® TiO<sub>2</sub> P25, used as the reference (Figure 5(c), and (d)). Of the samples fired at 450°C, the best one was the undoped titania. Its superior activity should be due to the concomitant presence of nanostructured anatase, brookite, and rutile (Ding *et al.*, 2000): to a certain extent, rutile, when nanostructured, is a visible-light active

photocatalyst (Yin *et al.*, 2004), since its band-gap is slightly shifted into the visible region, and, therefore, it has a higher visible light absorption compared to anatase. Moreover, brookite/rutile mixed systems have also recently been reported to be visible-light active photocatalysts (Pan *et al.*, 2009; Xu and Zhang, 2009). Considering the lower photocatalytic activity of the doped and co-doped samples in this case, we can infer that the dopants acted as electron-hole recombination centres. It can be seen that firing at 600°C clearly resulted in powders with a lower photocatalytic activity under visible light. At this firing temperature, the photocatalytic activity of the undoped sample dramatically decreased because, if on the one hand the crystallinity increased, on the other the excessive coarsening of the particles led to a huge decrease of its SSA (Table 2). The photocatalytic activity of the doped and co-doped samples followed the trend: W>W/Ag>Ag. Even though the relative anatase/rutile amounts in those samples are approximately the same, sample W-Ti600

**Table 2 . Band gap energy ( $E_g$ ) and specific surface area of pure, doped and co-doped titania**  
The energy band gap ( $E_g$ ) is calculated with the diffuse reflectance  $dR/d\lambda$  method

Sample	$E_g$ (eV)		$S_{BET}$ ( $m^2 g^{-1}$ )
	$dR/d\lambda$		
	rutile	Ag mid-gap contribution	
Ti450	3.06±0.01	–	41.9
W-Ti450	3.04±0.01	–	64.6
W/Ag-Ti450	3.07±0.02	2.93±0.02	47.5
Ag-Ti450	3.08±0.01	2.96±0.02	49.2
Ti600	3.03±0.01	–	4.0
W-Ti600	3.03±0.01	–	26.8
W/Ag-Ti600	3.08±0.01	2.93±0.02	22.7
Ag-Ti600	3.07±0.01	2.93±0.01	1.1

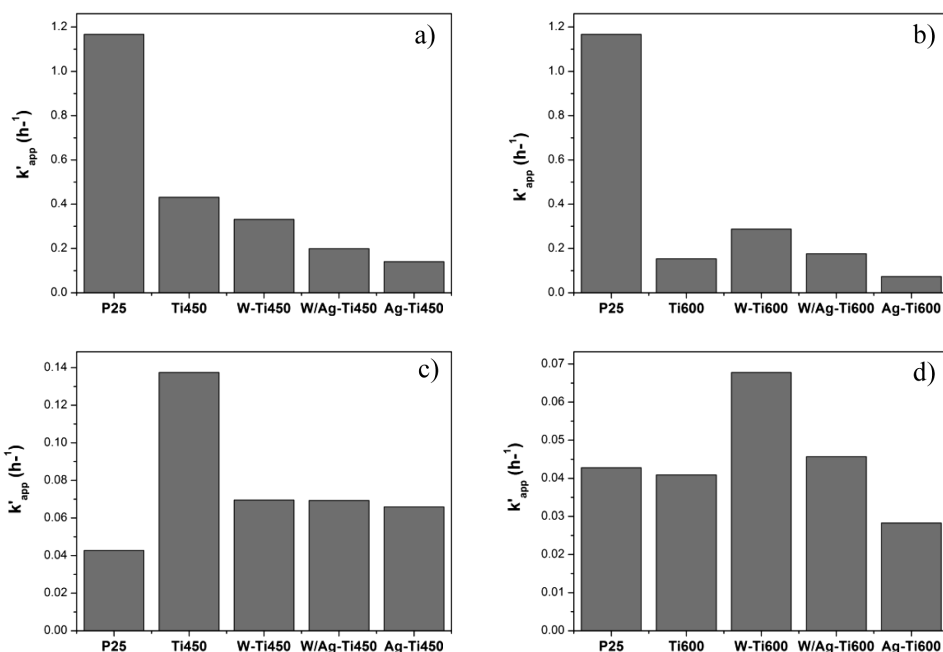


**Figure 5.** Photocatalytic degradation of methylene blue, considered as the apparent first-order constant ( $k_{app}$ ), assessed by: a) powders fired at 450°C, and: b) powders fired at 600°C, both under UVA exposure. Under visible-light exposure: c) powders fired at 450°C, and: d) powders fired at 600°C

(that possessing the highest SSA within the set of samples fired at 600°C) is once again the best performing photocatalyst, and the increase of the firing temperature did not dramatically affect its photocatalytic activity under visible-light exposure.

## Conclusions

Undoped titania and W-, Ag-, and W/Ag co-doped titanias were successfully synthesised via an aqueous sol-gel method. The simultaneous presence of rutile, anatase, and brookite was detected in the dried gels thermally treated at 450°C, together with a significant amount of amorphous phase. At 600°C, the only crystalline phases were anatase and rutile. Brookite recrystallised into rutile; tungsten addition was the more effective for delaying the ART.

The Ag- and co-doping gave the nanopowders a band gap contribution at around 2.93 eV (423 nm), due to the Ag

mid-gap localised levels. Undoped titania and the doped and co-doped powders, fired at 450°C, showed an appreciable photocatalytic activity under visible-light irradiation, better than the Aeroxide® TiO<sub>2</sub> P25 powder – without the need of any oxygen supply – due to the concomitant presence of nanostructured anatase and rutile. Tungsten doped and co-doped powders, at this firing temperature, were shown to be less photo-active than the undoped sample, probably due to the electron-hole recombination. At the highest firing temperature, 600°C, only the W-doped powder kept its high photocatalytic performance – not suffering from the increase in firing temperature – both under UVA and visible-light exposure.

## References

- Al-Ekabi, H. and Serpone, N. (1988). Kinetics studies in heterogeneous photocatalysis. I. Photocatalytic degradation of chlorinated phenols in aerated

- aqueous solutions over titania supported on a glass matrix. *J. Phys. Chem.-US*, 92:5,726-5,731.
- Arsac, F., Bianchi, D., Chovelon, J.M., Conchon, P., Ferronato, C., Lair, A., and Sleiman, M. (2008). Photocatalytic degradation of organic pollutants in water and in air. An analytical approach. *Mater. Sci. Eng. C*, 28:722-725.
- Augustynski, J. (1993). The role of the surface intermediates in the photoelectrochemical behaviour of anatase and rutile TiO<sub>2</sub>. *Electrochim. Acta*, 38:43-46.
- Chao, H.E., Yun, Y.U., Xingfang, H.U., and Larbot, A. (2003). Effect of silver doping on the phase transformation and grain growth of sol-gel titania powder. *J. Eur. Ceram. Soc.*, 23:1457-1464.
- Chen, J. and Poon, C.-S. (2009). Photocatalytic construction and building materials: from fundamentals to applications. *Build. Environ.*, 44:1899-1906.
- Choi, W., Termin, A., and Hoffmann, M.R. (1994). The role of metal ion dopants in quantum-sized TiO<sub>2</sub>: correlation between photoreactivity and charge carrier recombination dynamics. *J. Phys. Chem.*, 98:13669-13679.
- Di Paola, A., García-López, E., Ikeda, S., Marci, G., Ohtani, B., and Palmisano, L. (2002). Photocatalytic degradation of organic compounds in aqueous systems by transition metal doped polycrystalline TiO<sub>2</sub>. *Catal. Today*, 75:87-93.
- Ding, Z., Lu, G.Q., and Greenfield, P.F. (2000). Role of the crystallite phase of TiO<sub>2</sub> in heterogeneous photocatalysis for phenol oxidation in water. *J. Phys. Chem. B*, 104:4815-4820.
- Dubrovinsky, L.S., Dubrovinskaya, N.A., Swamy, V., Muscat, J., Harrison, N.M., Ahuja, R., Holm, B., and Johansson, B. (2001). Materials science. The hardest known oxide. *Nature*, 410:653-654.
- Fuente, A., Hernández-Alonso, M.D., Maira, A.J., Martínez-Arias, A., Fernández-García, M., Conesa, J.C., and Soria, J. (2001). Visible light-activated nanosized doped-TiO<sub>2</sub> photocatalyst. *Chem. Commun.*, 24:2718-2719.
- Fujishima, A. and Honda, K. (1972). Electrochemical photolysis of water at a semiconductor electrode. *Nature*, 238:37-38.
- Fujishima, A., Hashimoto, K., and Watanabe, T. (1999). *TiO<sub>2</sub> Photocatalysis: Fundamentals and Applications*. BKC, Inc., Tokyo, Japan, 126p.
- Fujishima, A., Rao, T.N., and Trick, D.A. (2000). Titanium dioxide photocatalysis. *J. Photochem. Photobiol. C*, 1:1-21.
- García-Serrano, J., Gómez-Hernández, E., Ocampo-Fernández, M., and Pal, U. (2009) Effect of Ag doping on the crystallization and phase transition of TiO<sub>2</sub> nanoparticles. *Curr. Appl. Phys.*, 9:1097-1105.
- Gualtieri A.F. and Brignoli, G. (2004). Rapid and accurate quantitative phase analysis using a fast detector. *J. Appl. Crystallogr.*, 37:8-13.
- Gualtieri, A.F. (2000). Accuracy of XRPD QPA using the combined Rietveld – RIR method. *J. Appl. Crystallogr.*, 33:267-278.
- Guo, M. and Du, J. (2012). First-principles study of electronic structures and optical properties of Cu, Ag, and Au-doped anatase TiO<sub>2</sub>. *Physica B*, 407:1003-1007.
- Haines, J. and Leger, J.M. (1993). X-ray diffraction study of TiO<sub>2</sub> up to 49 GPa. *Physica B*, 192: 233-237.
- Herrmann, J.-M., Duchamp, C., Karkmaz, M., Hoai, B.T., Lachheb, H., Puzenat, E., and Guillard, C. (2007). Environmental green chemistry as defined by photocatalysis. *J. Hazard. Mater.*, 146:624-629.
- Hoffmann, M.R., Martin, S.T., Choi, W., and Bahnemann, D.W. (1995). Environmental applications of semiconductor photocatalysis. *Chem. Rev.*, 95:69-96.
- Howard, C.J., Sabine, T.M., and Dickson, F. (1991). Structural and thermal parameters for rutile and anatase. *Acta Crystallogr.*, B47:462-468.
- Hutter, E., Fendler, J.H., and Roy, D. (2001). Surface plasmon resonance studies of gold and silver nanoparticles linked to gold and silver substrates by 2-aminoethanethiol and 1,6-hexanedithiol. *J. Phys. Chem. B*, 105:11159-11168.
- Jana, N.R., Sau, T.K., and Pal, T. (1999). Growing small silver particle as redox catalyst. *J. Phys. Chem. B*, 103:115-121.
- Jin, R., Cao, Y.C., Hao, H., M?traux, G.S., Schatz, G.C., and Mirkin, C.A. (2003). Controlling anisotropic nanoparticle growth through plasmon excitation. *Nature*, 425:487-490.
- Karvinen, S. and Lamminmäki, R.-J. (2003). Preparation and characterization of mesoporous visible-light-active anatase. *Solid State Sci.*, 5:1159-1166.
- Kominami, H., Murakami, S., Kato, J., Kera, Y., and Ohtani, B. (2002). Correlation between some physical properties of titanium dioxide particles and their photocatalytic activity for some probe reactions in aqueous systems. *J. Phys. Chem. B*, 106:10501-10507.
- Komornicki, S., Radecka, M., and Sobaś, P. (2004). Structural, electrical and optical properties of TiO<sub>2</sub>-WO<sub>3</sub> polycrystalline ceramics. *Mater. Res. Bull.*, 39:2007-2017.
- Kwon, Y.T., Song, K.Y., Lee, W.I., Choi, G.J., and Do, Y.R. (2000). Photocatalytic behaviour of WO<sub>3</sub>-loaded TiO<sub>2</sub> in an oxidation reaction. *J. Catal.*, 191:192-199.
- Lansdown, A.B.G. (2010). Silver in Healthcare: Its Antimicrobial Efficacy and Safety in Use.

- 1<sup>st</sup> ed. Royal Society of Chemistry, Cambridge, UK, 280p.
- Larson, A.C. and Von Dreele, R.B. (2000). General Structure Analysis System (GSAS). Los Alamos National Laboratory Report LAUR 86-784, Los Alamos, NM, USA.
- Li, X.Z., Li, F.B., Yang, C.L., and Ge, W.K. (2001). Photocatalytic activity of  $\text{WO}_x\text{-TiO}_2$  under visible light irradiation. *J. Photoch. Photobio. A*, 141:209-217.
- Malato, S., Fernández-Ibáñez, P., Maldonado, M.I., Blanco, J., and Gernjak, W. (2009). Decontamination and disinfection of water by solar photocatalysis: recent overview and trends. *Catal. Today*, 147:1-59.
- Marfunin, A.S. (1979). *Physics of Minerals and Inorganic Materials. An Introduction*, Springer-Verlag, Berlin, Germany, 340p.
- Meagher, E.P. and Lager, G.A. (1979). Polyhedral thermal expansion in the  $\text{TiO}_2$  polymorphs: refinement of the crystal structures of rutile and brookite at high temperature. *Can. Mineral.*, 17:77-85.
- Muscat, J. Swamy, V., and Harrison, N.M. (2002). First-principles calculations of the phase stability of  $\text{TiO}_2$ . *Phys. Rev. B*, 65:224112
- Ohno, T., Sarukawa, K., and Matsumura, M. (2001). Photocatalytic activities of pure rutile particles isolated from  $\text{TiO}_2$  powder by dissolving the anatase component in HF solution. *J. Phys. Chem. B*, 105:2417-2420.
- Okada, K., Yamamoto, N., Kameshima, Y., Yasumori, A., and Mac Kenzie, K.J.D. (2001). Effect of silica additive on the anatase-to-rutile phase transition. *J. Am. Ceram. Soc.*, 84:1591-1596.
- O'Regan, B. and Grätzel, M. (1991). A low-cost, high-efficiency solar cell based on dye-sensitized colloidal  $\text{TiO}_2$  films. *Nature*, 353:737-749.
- Pan, H., Qiu, X., Ivanov, I.N., Meyer, H.M., Wang, W., Zhu, W., Parans Paranthaman, M., Zhang, Z., Eres, G., and Gu, B. (2009). Fabrication and characterization of brookite-rich, visible light-active  $\text{TiO}_2$  films for water splitting. *Appl. Catal. B-Environ.*, 93:90-95.
- Puddu, V., Choi, H., Dionysiou, D.D., and Li Puma G. (2010).  $\text{TiO}_2$  photocatalyst for indoor air remediation: influence of crystallinity, crystal phase, and UV radiation intensity on trichloroethylene degradation. *Appl. Catal. B-Environ.*, 94:211-218.
- Sakthivel, S., Shankar, M.V., Palanichamy, M., Banumathi, A., Bahnemann, D.W., and Murugesan, V. (2004). Enhancement of photocatalytic activity by metal deposition: characterisation and photonic efficiency of Pt, Au and Pd deposited on  $\text{TiO}_2$  catalyst. *Water Res.*, 38:3001-3008.
- Sato, H., Endo, S., Sugiyama, M., Kikegawa, T., Shimomura, O., and Kusaba, K. (1991). Baddeleyite-type high-pressure phase of  $\text{TiO}_2$ . *Science*, 251: 786-788.
- Sclafani, A. and Herrmann, J-M. (1998). Influence of metallic silver and of platinum-silver bimetallic deposits on the photocatalytic activity of titania (anatase and rutile) in organic and aqueous media. *J. Photoch. Photobio. A*, 113:181-188.
- Serpone, N., Lawless, D., Disdier, J., and Herrmann, J-M. (1994). Spectroscopic, photoconductivity, and photocatalytic studies of  $\text{TiO}_2$  colloids: naked and with the lattice doped with  $\text{Cr}^{3+}$ ,  $\text{Fe}^{3+}$ , and  $\text{V}^{5+}$  cations. *Langmuir*, 10:643-652.
- Shannon, R.D. (1976). Revised effective ionic radii and systematic studies of interatomic distances in halides and chalcogenides. *Acta Crystallogr.*, A32:751-767.
- Tatsuma, T., Saitoh, S., Ohko, Y., and Fujishima, A. (2001).  $\text{TiO}_2\text{-WO}_3$  photoelectrochemical anticorrosion system with an energy storage ability. *Chem. Mater.*, 13:2838-2842.
- Tobaldi, D.M., Tucci, A., Sever Škapin, A., and Esposito, L. (2010). Effects of  $\text{SiO}_2$  addition on  $\text{TiO}_2$  crystal structure and photocatalytic activity. *J. Eur. Ceram. Soc.*, 30:2,481-2,490.
- Toby, B.H. (2001). EXPGUI, a graphical user interface for GSAS. *J Appl. Crystallogr.*, 34:210-213.
- Wang, Y. and Herron, N. (1991). Nanometer-sized semiconductor clusters: materials synthesis, quantum size effects, and photophysical properties. *J. Phys. Chem.*, 95:525-532.
- Weir, A., Westerhoff, P., Fabricius, L., Hristovski, K., and von Goetz, N. (2012). Titanium dioxide nanoparticles in food and personal care products. *Environ. Sci. Technol.*, 46:2242-2250.
- Xu, H. and Zhang, L. (2009). Controllable one-pot synthesis and enhanced photocatalytic activity of mixed-phase  $\text{TiO}_2$  nanocrystals with tunable brookite/rutile ratios. *J. Phys. Chem. C*, 113:1785-1790.
- Yin, S., Hasegawa, H., Maeda, D., Ishitsuka, M., and Sato, T. (2004). Synthesis of visible-light-active nanosize rutile titaniaphotocatalyst by low temperature dissolution-precipitation process. *J. Photoch. Photobio. A*, 163:1-8.
- Zhang, H. and Banfield, J.F. (2000). Understanding polymorphic phase transformation behaviour during growth of nanocrystalline aggregates: insights from  $\text{TiO}_2$ . *J. Phys. Chem. B*, 104: 3481-3487.